Behavioral PAM-4 VCSEL Model using Stochastic Multimode Rate Equations for Link Design Optimization

Alirio Melgar[1], V. A. Thomas[1], Benjamin D.B. Klein[2], Itshak Kalifa[3], Paraskevas Bakopoulos[3], Elad Mentovich[3] and Stephen E. Ralph[1]

[1]*Department of Electrical and Computer Engineering, Georgia Institute of Technology, Atlanta, Georgia, USA*
stephen.ralph@ece.gatech.edu

[2]*Department of Electrical and Computer Engineering, Kennesaw State University, Kennesaw, Georgia, USA*
bklein8@kennesaw.edu

[3]*Nvidia Networking, Hakidma 26 Ofer Industrial Park, Yokneam, Israel*
itsikk@nvidia.com

Abstract: A stochastic multimode laser model aimed at optimizing optical links is proposed. The model simulates experimental results from commercial VCSELs and depicts transverse mode effects that are increasingly important in high-speed PAM-4 links. © 2022 The Author(s)

1. Introduction

As demand for higher data rates increases, vertical cavity surface emitting lasers (VCSELs) remain a popular choice for high-speed, short reach communications. Here, we present the results of a parameter extraction technique first proposed by us in [1] that relies on both the RIN spectrum and modulation response to characterize multimode VCSEL parameters. We demonstrate that our stochastic VCSEL model is capable of accurately simulating both frequency- and time-domain characteristics in PAM-4 VCSEL optical links, while incorporating both bandwidth and noise limitations and supporting large signal simulations such as PAM-4. Models such as these are necessary for next generation optical links powered by equalization, pulse shaping and multilevel modulation formats.

2. Behavioral Laser Model

VCSEL laser dynamics are modeled by a set of coupled rate equations. These equations describe the relation between the carrier density N and photon density S. The multimode-mode laser rate equations are [1,2]

$$\frac{dN}{dt} = \frac{\eta_i I_{out}}{qV} - \frac{N}{\tau_n} - \sum_m v_{gm} G_m S_m + F_N(t) \tag{1}$$

$$\frac{dS_m}{dt} = -\frac{S_m}{\tau_{pm}} + \Gamma_m R'_{spm} + \Gamma_m v_{gm} G_m S_m + F_{Sm}(t) \tag{2}$$

where v_{gm} is the group velocity and Γ_m is the confinement factor (i.e. the ratio of the active region volume V of the carrier reservoir to the m^{th} mode volume V_{pm} of the photon reservoir). Optimizable parameters are defined in Table 1 with a representative set of values and a corresponding frequency response shown in Fig 1. Here, R'_{spm} is the fraction of the spontaneous emission that lases into the m^{th} mode of interest

$$R'_{spm} = \frac{v_{gm} G_m n_{spm}}{V_{pm}} \tag{3}$$

where n_{spm} is the population inversion factor typically between 1 and 2. Less common is the inclusion of $F_N(t)$ and $F_{S_m}(t)$, the Langevin noise sources that account for relative electron and photon noise sources and that produce intensity noise (RIN). Langevin noise source spectral densities have been added to the model through the addition of the following correlations:

$$\langle F_N F_N \rangle = \frac{\eta_i I}{qV^2} + \sum_m 2R'_{spm} S_m - \sum_m \frac{v_{gm} G_m S_m}{V} \tag{4}$$

$$\langle F_N F_{S_m} \rangle = -2R'_{spm} S_m + \frac{v_{gm} G_m S_m}{V_{pm}} \tag{5}$$

$$\langle F_{S_m} F_{S_m} \rangle = 2\Gamma_m R'_{spm} S_m \tag{6}$$

$$\langle F_{S_m} F_{S_n} \rangle|_{m \neq n} = 0 \tag{7}$$

The details and mathematical modeling of noise sources have been discussed previously in [1]. The gain-carrier density relation experienced by each mode in a quantum well is modeled by

$$G_m = \frac{g_o}{1 + \sum_n \epsilon_{mn} S_n} ln\left(\frac{N + N_s}{N_s + N_t}\right) \tag{8}$$

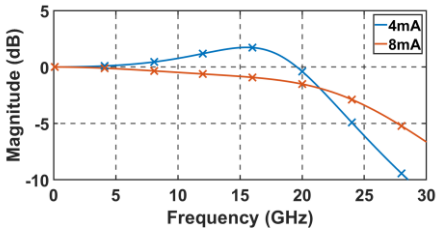

Fig. 1. Test VCSEL of Table 1: Example S21 using VCSEL parameters from Table 1.

Table I. Typical VCSEL Parameters	
Laser Parameters	**Test VCSEL**
injection efficiency η_i	0.7
photon lifetime (ps) $[\tau_{p1}, \tau_{p2}, \tau_{p3}] = \tau_p$	3
gain coeff (cm^{-1}/s) g_o	3x10^4
carrier lifetime (ns) τ_n	2.5
gain linearity parameter (cm^{-3}) N_s	3x10^{18}
carrier density at transparency (cm^{-3}) N_{tr}	1x10^{18}
gain comp. coeff. (cm^3) $[\epsilon_{11}, \epsilon_{22}, \epsilon_{33}] = \epsilon$	4x10^{-16}
mode volume (cm^3) $[V_{p1}, V_{p2}, V_{p3}] = V_p$	[0.63,0.63,0.63] x10^{-10}

where N_t is carrier density at transparency and N_s is a linearity parameter used to determine the shape of the gain. We model all the gain compression terms in a 3-mode scenario as a matrix where the diagonal elements represent self-saturation, and off-diagonal elements represent cross-saturation. In VCSELs, it has been shown that the modal overlap and hence the cross-gain saturation between adjacent modes is significantly greater than non-adjacent modes [3,4]. For the case of equal optical power in 3 modes, we chose the following matrix structure that meets all the previously mentioned criteria

$$\epsilon_{mn} = \begin{bmatrix} \epsilon(1-x) & x\epsilon & 0 \\ x\epsilon & \epsilon(1-2x) & x\epsilon \\ 0 & x\epsilon & \epsilon(1-x) \end{bmatrix} \tag{9}$$

where x varies between 0 and 0.5 and represents the overlap between modes. It allows us to vary the degree of cross and self-gain saturation, while ensuring that all elements remain non-negative. While there are multiple possible candidate structures, the formulation in equation (7) is simple and accurately captures the desired effects.

3. Mode Noise Correlations

By systematically enabling/disabling Languevin noise sources we can establish that the main Langevin correlations accounting for the RIN cross correlations are the $\langle F_{S_m} F_{S_m} \rangle$ terms. While photon Langevin correlations $\langle F_{S_m} F_{S_m} \rangle$ are largely dependent on G_m and S_m, steady state solutions show that S_m can be directly tuned using G_m. Hence, one can conclude that RIN cross correlations originate at the photon level in the gain region, and that the carrier pool acts as a medium through which these photon reservoirs interact, primarily through hole burning.

Historically RIN cross correlations have been modeled by setting $x = 0$, which assumes zero cross gain saturation due to no or weak mode overlaps. Thus, generating strictly negative RIN cross correlations. However, both positive and negative RIN cross correlations were experimentally measured in [3]. Figures 2a and 2b shows the RIN cross correlations and temporal behavior when the VCSEL experiences cross gain saturation between the modes i.e., $x > 0$. Here, we see that the lack of cross gain saturation, from (9), between modes 1 and 3, leads to a positive noise correlation between these modes. Further evaluation shows that as the mode experiences higher and higher gain saturation, the correlation time with other modes is increased. Furthermore, as the mode experiences more gain saturation it takes longer for the saturated mode to react to changes from other modes which elongates the correlation time. One can also note that the correlation times are longer at lower bias current conditions. This is likely due to the spontaneous emission into the lasing mode being a larger fraction of the total power at lower bias currents. These trends can also be seen in the temporal waveforms of Fig. 2b. The negative correlations between modes 1-2 and 2-3

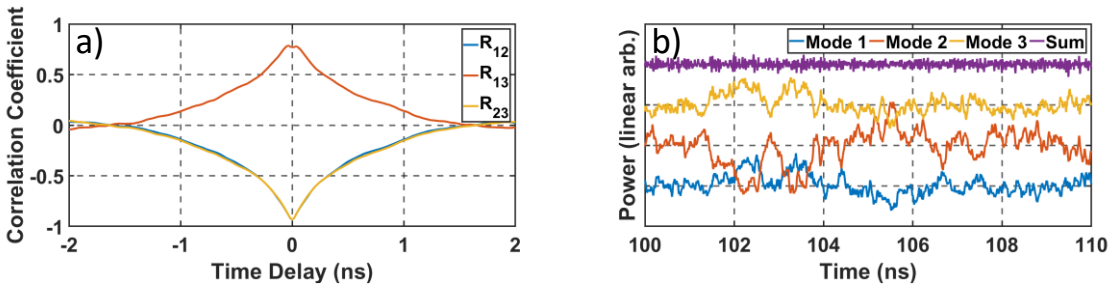

Fig. 2. Test VCSEL parameters of Table 1: (a) Cross correlations at 8mA for x=0.32. The magnitude of the correlation coefficient and time correlation increases with increasing cross correlation. (b) Temporal output from stochastic rate equation at 8mA for x=0.32. Modes have been artificially shifted for clarity. Note that if all power is captured, total noise is significantly lower than individual modes.

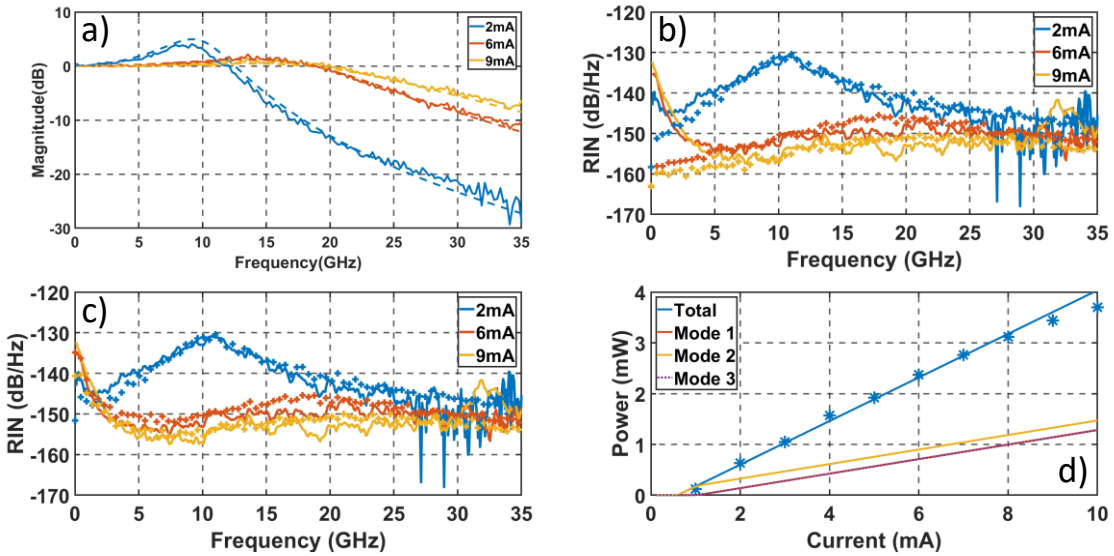

Fig. 3. Comparison between measured (solid) and simulation (dotted) for a) small signal frequency response b) RIN w/o spatial filtering c) RIN w/ spatial filtering and positive/negative correlations d) LI curve, experimental data is shown as blue dots.

along with the positive correlation between modes 1-3 become increasingly pronounced as x increases.

4. Experimental Results

Figure 3 and 4 shows results using our experimental test bed. Our setup includes a Keysight M8196A and 86100D scope. S_{21} data was taken with an Agilent 8530A VNA. The VCSEL under test is part of a 1x4 Nvidia VCSEL array designed for use in high-speed data communication parallel applications. The 28Gbaud 850nm GaAs/InGaAs QW VCSELs were measured to have a bandwidth of ~26.5GHz at 9mA (Fig 3a), with a measured thermal roll over of ~13mA. Before data acquisition, the components which include the AWG, bias-T, detector, amplifier, and scope were equalized out. Figure 4 depicts experimental and simulated eye diagrams at 52 and 92Gpbs. Highest bitrate achieved is limited by AWG bandwidth.

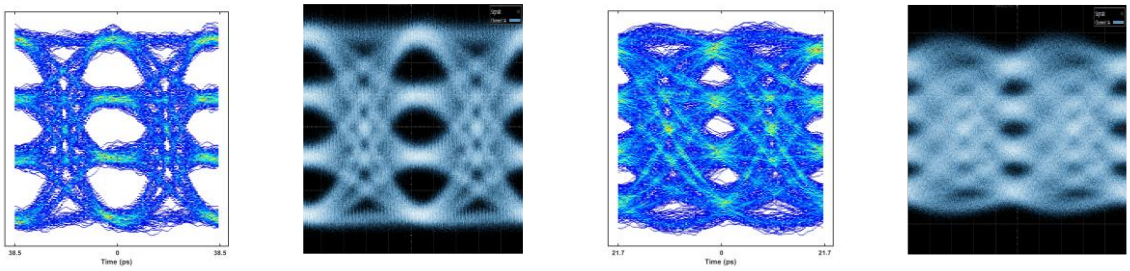

(a) (b) (c) (d)

Fig. 4. Simulated (a,c) and experimentally measured (b,d) PAM-4 eye diagrams at 52Gbps (a,b) and 92 Gbps (c,d)

5. References

[1] A. Melgar, V. A. Thomas and S. E. Ralph, "Multi-Objective Laser Rate Equation Based Parameter Extraction Using VCSEL Small Signal Response and RIN Spectra," in Journal of Lightwave Technology, vol. 38, no. 23, pp. 6437-6445, 2020

[2] L. A. Coldren and S. W. Corzine, Diode lasers and photonics integrated circuits, John Wiley Sons, New York, USA, 1995.

[3] J. Lavrencik, S. Kota Pavan, V. A. Thomas and S. E. Ralph, "Noise in VCSEL-Based Links: Direct Measurement of VCSEL Transverse Mode Correlations and Implications for MPN and RIN," in Journal of Lightwave Technology, vol. 35, no. 4, pp. 698-705, 2017

[4] J. Y. Law and G. P. Agrawal, "Mode-partition noise in vertical-cavity surface-emitting lasers," in IEEE Photonics Technology Letters, vol. 9, no. 4, April 1997